Composition dependence of the charge-driven phase transition in group-VI transition metal dichalcogenides

Urvesh Patil and Nuala M. Caffrey[*]

School of Physics and CRANN, Trinity College, Dublin 2, Ireland

Materials exhibiting multiple stable phases can be used as functional components in electronic and optical applications if the phase transition is controllable. Group-VI transition metal dichalcogenides (TMDs, MX_2, where M = Mo, W and X = S, Se) are known to undergo charge induced transitions from semiconducting H phases to metallic T phases. This occurs, for example, when bulk TMDs are exfoliated with the aid of alkali ion intercalants. However, it is difficult to experimentally decouple the effect of composition-dependent phase transition barriers from indirect effects related to the exfoliation process. Here, using first-principles calculations, we study the energetics of transition between the different structural polytypes of four group-VI TMDs upon lithium adsorption. We find that both the activation barrier from the H phase to the metallic phase in charged monolayers and the reverse barrier in neutral monolayers are required to explain experimental results. We show that the high proportion of metallic phase found in WS_2 monolayers after alkali treatment can be explained by high transition barriers to revert back to the H phase once in a neutral state. The calculated barriers however cannot explain the low proportion of metallic phase found in MoS_2 monolayers in some experiments and so nonelectronic effects must also play a role.

I. INTRODUCTION

Transition metal dichalcogenides (TMDs), comprised of layered sheets of transition metal atoms sandwiched between two layers of chalcogen atoms (MX_2), are chemically versatile, exhibiting a broad range of electronic properties from insulating (ZrS_2) to superconducting ($NbSe_2$) [1]. As well as by changing the composition, the conductivity of a TMD can be modified by inducing a structural transition between different polymorphs. Several such polymorphs exist, distinguished by the metal coordination of the chalcogen atoms. In the semiconducting H phase, the chalcogen atoms are AA stacked so that the metal atoms occupy alternate trigonal-prismatic voids. The metallic T phase, on the other hand, has a tetragonal symmetry, with the metal atoms occupying octahedral voids between AB-stacked chalcogen atoms. This particular phase can transform to a semimetallic distorted octahedral phase, designated here as T'. Recently, a further mixed phase, designated T'', which can be viewed as a series of alternating H and T' phases, was theoretically predicted to be lower in energy than the T' phase for MoS_2 [2].

The ability to induce a transition in MoS_2 from its ground state H phase to an octahedral phase via alkali metal intercalation has been known since the 1980s [3]. This phase transition was attributed to a transfer of charge from the intercalated atom to the TMD, and more specifically to the d states of the transition metal atom [4,5]. Indeed, the entire family of group-VI TMDs, where M = Mo, W and X = S, Se, and Te, can be manipulated to undergo phase transitions close to ambient conditions [6]. This has been achieved using a variety of methods, including alkali metal adsorption [3,7–9], the introduction of impurities or vacancies [10–12], electron or laser irradiation [11,13–17], and electrostatic gating [18,19].

The electronic properties of a TMD are evidently strongly dependent on its structural phase. In MoS_2 the conductivity of the T phase was found to be up to 10^7 times higher than that of the semiconducting H phase [20]. The ability to reversibly and reliably switch between these two phases would result in applications as monolayer-thick field effect transistors [21], gas sensors [22], and catalysts [23]. Such applications require precise control over the phase transition process so that a complete phase change to T' phase can be achieved and maintained.

Liquid phase exfoliation, with the aid of alkali metal intercalation, is a common and effective way of isolating TMD monolayers from the bulk on an industrial scale. In such experiments, the alkali metal atoms are first intercalated into the bulk TMD using an organolithium compound. The intercalated TMD is then solvated in a polar solvent. This results in the discharging of the monolayers, the deintercalation of the metal ion, and the exfoliation of individual monolayers from the bulk materials. These layers are subsequently measured to have both H and T phases present.

Of the group-VI TMDs, the phase transition in MoS_2 has been investigated in detail. Yet, compared to other group-VI TMDs, the phase transition efficiency in MoS_2 can be relatively low: a comprehensive side-by-side comparison of the experimental transition efficiency in four group-VI TMDs—MoS_2, $MoSe_2$, WS_2, and WSe_2—found that WS_2 exhibited the largest increase in the proportion of the $1T$ phase compared to the starting $2H$ phase (i.e., the $1T/2H$ ratio), followed by $MoSe_2$ and WSe_2, and eventually MoS_2 [24].

*nuala.caffrey@tcd.ie

While the exact ratios were subsequently found to depend on the nature of the organolithium intercalant group used in the experiment, the general trend remained: WX_2 compounds display a higher proportion of T phase compared to MoX_2, for both X = S and Se [25,26].

In these alkali metal induced exfoliation experiments, the measured phase transition efficiency will depend not only on the intrinsic composition-dependent free-energy barrier between the different phases, but also on the composition-dependent exfoliation efficiency of the chosen organolithium intercalant. Experimentally, it is difficult to decouple these two contributions. As ion-assisted liquid phase exfoliation is the most suitable method of producing sufficient T phase TMDs on an industrial scale, a complete understanding of the mechanism is essential to maximize the amount of metallic phase produced and to prevent a transition back to the H phase.

Previous computational investigations of the phase transition barrier have concentrated on MoS_2, looking primarily at the threshold charge density required to induce the phase transition. However, a disconcertingly wide range of values have been reported, including 0.35 [27], 0.55 [2], 0.78 [28], and almost $2e$/f.u. [29]. The origin of this discrepancy is discussed in detail in the Appendix.

Here, using first-principle calculations, we determine the transition barriers between all possible polytypes of both the pristine and Li-adsorbed group-IV TMDs, with the aim of determining whether the composition dependence of experimental transition efficiency in four group-VI TMDs can be explained using the intrinsic barriers to the phase transitions alone.

II. COMPUTATIONAL METHODS

Density functional theory (DFT) calculations are performed using the VASP-5.4 code [30–32]. The optB86b-vdW exchange-correlation functional was used to account for long range dispersion interactions [33,34]. This functional was previously shown to give accurate lattice parameters and energies for layered materials [35,36]. All calculations are performed with a cutoff energy of 500 eV for the plane wave basis set. A Γ centered K-point grid of $11 \times 7 \times 1$ is used to calculate the total energy of the H and T' phases, while a $11 \times 5 \times 1$ grid is used for the T'' mixed phase.

The structures are relaxed until the force on each atom is less than 0.01 eV/Å. The unit cell length in the direction normal to the plane is fixed at 25 Å for H and T' phase calculations, and 26 Å for T'' mixed phase calculations and all transition state calculations. This corresponds to a minimum vacuum of 18 Å between repeating monolayers and the dipole corrections are applied.

The climbing image nudged elastic band (CI-NEB) method is used to determine the transition barrier between two different phases [37,38]. This method involves a constrained geometry optimization of a series of interpolated structures between the two stable phases connected by springs with a spring constant of 5 eV/Å^2. The springs prevent the interpolated structures from converging to the nearest stable phase. All atoms in the transition state calculations are optimized so that the force on each atom is less than 0.05 eV/Å.
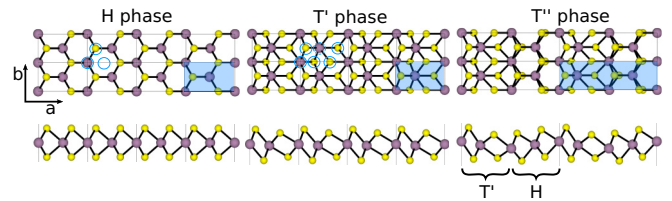
FIG. 1. Top and side view of the H, T', and T'' polytypes. The orthorhombic cells of all three phases are shown as blue shaded regions. Note that the T'' mixed phase can be viewed as alternating T' and H phases. The blue circles indicate the possible candidate sites for lithium adsorption.

III. RESULTS

A. Neutral monolayers

The crystal structures of the H, T', and T'' mixed phases are shown in Fig. 1. The structural parameters determined for all neutral monolayers (without adsorbed Li) are given in Table I. The lattice constants are dictated by the chalcogen atom, with MoS_2 and WS_2 having very similar values in all three phases. Likewise, $MoSe_2$ and WSe_2 have almost identical lattice constants. These values are in good agreement with the available experimental data [39–48] and with previous calculations [49–52] in the literature. For the T' phase, the calculated a lattice constant of 5.57 Å for MoS_2 is consistent with the experimentally observed length of 5.6 Å.

In agreement with previous DFT studies, we find the H phase to be the ground state structure for all four materials [11,19,28,29,53–55]. The total energy differences between this phase and both the T' phase and the T'' mixed phase are given in Fig. 2. We find that the energy difference between the H phase and the T' phase is larger for the sulfides compared to the selenides. It reduces from 0.57 eV for MoS_2 to 0.35 eV for $MoSe_2$ and from 0.56 eV for WS_2 to 0.29 eV for WSe_2. Similarly, the energy difference between the H phase and the T'' mixed phase reduces from 0.49 eV for MoS_2 to 0.35 eV for $MoSe_2$ and from 0.52 eV for WS_2 to 0.35 eV for WSe_2. While the H phase is the ground state in all four cases, the T' phase is energetically more favorable than the T'' mixed phase for WSe_2 but the ordering is opposite for the MoS_2 and WS_2 (the difference is negligible for $MoSe_2$).

The activation barriers to induce a phase transition from the H phase to the T' and T'' mixed phases, as calculated with the CI-NEB method, for all four materials are also shown in Fig. 2. In all cases, the energy barrier to transition

TABLE I. The lattice parameters a, b (in Å) of the H, the T', and the T'' mixed phase of MoS_2, $MoSe_2$, WS_2, and WSe_2.

	H		T'		T''	
	a	b	a	b	a	b
MoS_2	5.48	3.16	5.57	3.22	11.23	3.16
$MoSe_2$	5.71	3.30	5.79	3.34	11.69	3.27
WS_2	5.48	3.17	5.59	3.23	11.24	3.18
WSe_2	5.71	3.30	5.81	3.35	11.69	3.28
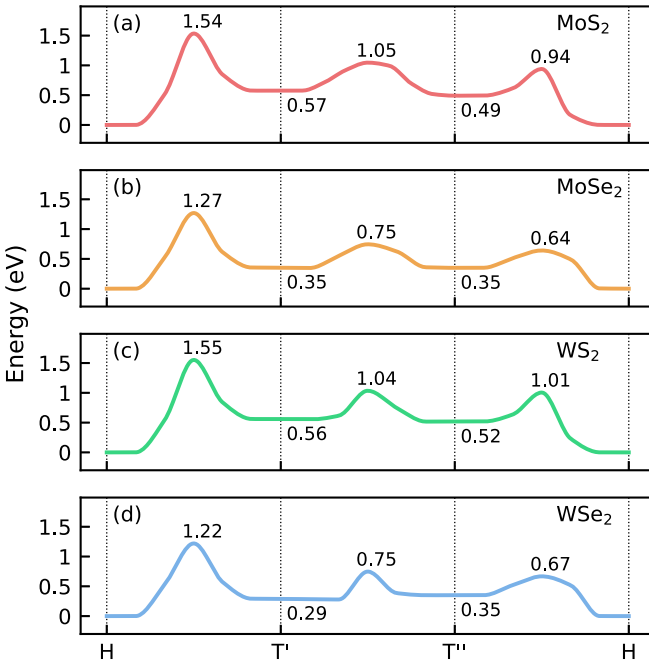
FIG. 2. The relative energy difference and transition barrier between the H phase, the T' phase, and the T'' mixed phase of (a) MoS_2, (b) $MoSe_2$, (c) WS_2, and (d) WSe_2. Energies are referred to that of the H phase for each material.

directly from the H phase to the T' phase is large, ranging between 1.22 and 1.54 eV. In general, the barrier is smaller for MSe_2 than for MS_2. The energy barrier to transition from the H phase to the T'' mixed phase is smaller, ranging between 0.64 and 1.01 eV. Again, the smallest values occur for the MSe_2 compounds. In all cases the energy barrier to transition from the ground state H phase to the lowest-lying T phase (namely, T'' for MoS_2, $MoSe_2$, and WS_2, and T' for WSe_2) lies between 0.64 and 1.22 eV. Evidently, the H phase is very stable and will not convert to the T phase spontaneously, in agreement with experiment. Note that the transition from the T' phase to the T'' mixed phase requires the conversion of only half of the lattice from the T' phase to the H phase while keeping the other half fixed. Consequently, the barrier to transition from the T' phase to the T'' mixed phase is lower (by between 50% and 65%) than the barrier to undergo the complete transition from T' phase to the H phase.

The calculated barriers reported here are in units of eV per formula unit (MX_2) to facilitate comparison between four materials and the total activation energy required for transition will scale with the number of formula units which transition simultaneously [17]. Note that the phase transition between the H phase and the T phase was shown to be diffusive, rather than a simultaneous phase transition of the entire monolayer. As a result, the activation barrier per formula unit will be modified by the exact details of the nucleation process.

B. Charged monolayers

Introducing extra charge to the TMD via an interaction with explicitly modeled strong donor atoms bypasses issues related to static charging (discussed in the Appendix). We consider two different concentrations of Li atoms adsorbed on the surface of the monolayers, namely $Li_{0.5}MX_2$ and Li_1MX_2. The stability of the alkali metal-adsorbed monolayer decreases at higher concentrations, and eventually becomes unstable for $Li_{1.5}MX_2$, in agreement with experiment [56–58].

The adsorption sites were determined by calculating the total energy of lithium adsorbed on all of the unique candidate sites, shown as blue circles in Fig. 1. These sites include those directly on top of the metal atom, on top of the chalcogen atoms, and on the hollow site. In agreement with previous calculations in the literature [59], we find that irrespective of the material or phase the lowest energy adsorption site is on top of the metal atom. (The preferred adsorption position on the T' phase is shown with a dashed circle in Fig. 1.) When increasing the Li concentration to $LiMX_2$, the second Li atom per unit cell adsorbs on the opposite surface, minimizing the electrostatic interaction between the two Li atoms. This configuration is 0.1 eV/f.u. lower in energy than that with both Li atoms adsorbed on the same side of the monolayer. For the case of the T'' mixed phase, the lithium atoms are also positioned on top of the metal atoms. For $Li_{0.5}MX_2$, one lithium atom is placed in the H phase region and another in the T' phase region. For Li_1MX_2, the remaining lithium atoms were placed on top the metal atoms on the opposite side of the slab. The adsorption on opposite surfaces is consistent with a uniform intercalation in the bulk material [16].

The extra charge introduced by the Li atoms causes an expansion of the TMD lattice constants. These values are given in Table II. A Li concentration of $Li_{0.5}MX_2$ increases the lattice constants of the H phase by between 0.3% and 1.75% compared to the neutral lattice. Similarly, Li adsorption increases the lattice constants of the T' phase by between

TABLE II. The lattice parameters a, b (in Å) of the H, the T', and the T'' mixed phase of $Li_{0.5}MX_2$ and $LiMX_2$ in the orthorhombic unit cell.

| | $Li_{0.5}MX_2$ | | | | | | $LiMX_2$ | | | | | |
| | H | | T' | | T'' | | H | | T' | | T'' | |
	a	b	a	b	a	b	a	b	a	b	a	b
MoS_2	5.53	3.19	5.75	3.25	11.49	3.20	5.68	3.23	5.9	3.29	11.79	3.22
$MoSe_2$	5.8	3.32	6.	3.37	11.95	3.34	5.98	3.36	6.12	3.46	12.2	3.38
WS_2	5.51	3.18	5.74	3.26	11.47	3.19	5.98	3.36	5.88	3.27	11.72	3.19
WSe_2	5.81	3.29	5.97	3.4	11.90	3.33	5.94	3.33	6.06	3.47	12.30	3.33
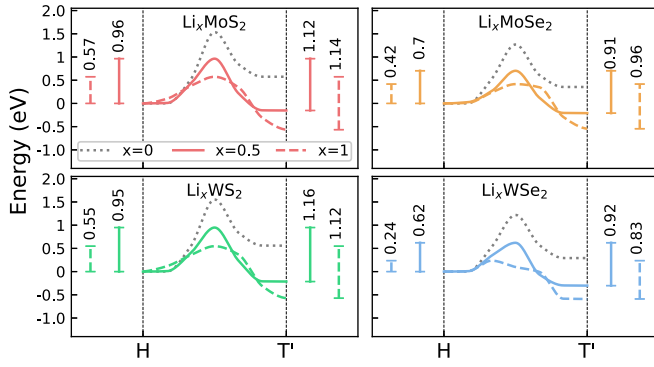
FIG. 3. The relative energy difference and transition barrier between the H phase and the T' phase of Li_xMoS_2, Li_xMoSe_2, Li_xWS_2, and Li_xWSe_2 with $x = 0$ (dotted line), $x = 0.5$ (solid line), and $x = 1$ (dashed line). The segments on the left (right) of the curves indicate the barrier for transition from the H to T' (T' to H) phase. Energies are referred to that of the H phase of each material.

0.9% and 3.23%. Increasing the lithium concentration causes the lattice to expand further, and the expansion is higher in the selenides compared to the sulfides. Bader charge analysis [60] finds that, for both concentrations considered here, each Li atom donates approximately $0.82e$/f.u. This value is independent of the material type and phase, indicating that the nature of the interaction is similar.

The energy differences between the different polytypes, for all four compounds and for both Li concentrations, are summarized in Fig. 3. The T' phase becomes the ground state structure of all four Li-adsorbed TMDs. This is followed by the H phase and finally the T'' mixed phase. This is in agreement with previous studies on MoS_2 which have shown a phase transition to occur at a Li concentration of $Li_{0.4}MoS_2$ [61], a K concentration of $K_{0.225}WSe_2$ [9], and a Na concentration of $Na_{0.375}MoS_2$ [57].

The energy difference between both the T' and T'' mixed phases compared to the H phase increases going down the group from S to Se and also going from Mo to W for both considered Li concentrations. On increasing the lithium concentration from $Li_{0.5}MX_2$ to Li_1MX_2, the energy difference between the T'' mixed phase and the H phase decreases slightly for the sulfides but increases for the selenides. In contrast to our observation that the energy of the T'' mixed phase increases with respect to the H phase, Ma *et al.* reported a threshold of $0.4e$ per MoS_2 to induce the transition from the H phase to the T'' mixed phase [2]. This discrepancy could be a consequence of the static charging method used in obtaining those results.

These trends in stability can be explained by simple electron filling in the rigid band approximation [9]. For the H and T'' mixed phases, excess electrons cause an increase in total energy equal to the band gap. As the T' phase is semimetallic, the next available energy level is at the Fermi level, and so this phase becomes lower in energy.

The barriers for the H to T' phase transition in the charged monolayers are also shown in Fig. 3. In all cases, the barrier for the phase transition decreases due to lithium adsorption. The maximum barrier for the transition from the H phase to the T' phase is found for MoS_2 at a value of 0.96 eV

TABLE III. Adsorption energy E_{ads} of lithium on the H and T' TMD phases (eV per unit MX_2).

	$Li_{0.5}MX_2$		$LiMX_2$	
	E_{ads}^{H}	$E_{ads}^{T'}$	E_{ads}^{H}	$E_{ads}^{T'}$
MoS_2	−0.97	−1.64	−2.51	−3.24
$MoSe_2$	−0.99	−1.41	−2.36	−2.89
WS_2	−0.85	−1.58	−2.26	−2.98
WSe_2	−1.03	−1.38	−2.16	−2.70

for $Li_{0.5}MoS_2$ and 0.57 eV for $Li_{0.5}MoS_2$. The minimum transition barrier from the H phase to the T' phase is found for WSe_2 with a barrier of 0.62 eV for $Li_{0.5}WSe_2$ and 0.24 eV for Li_1WSe_2. WS_2 has the second highest barrier, at a value of 0.55 eV for the Li_1WS_2 structure, while $MoSe_2$ has a barrier of 0.42 eV at the same Li concentration. In all cases, the barrier to transition does not decrease to zero. As such, the transition cannot be spontaneous and an energy equal to the barrier height needs to be provided to induce the transition.

IV. DISCUSSION

Li adsorption is an exothermic process. The adsorption energies, defined as $E_{ads} = E_{Li_xMX_2} - E_{MX_2} - xE_{Li}$ where $E_{Li_xMX_2}$ is the total energy of the Li adsorbed structure, E_{MX_2} is the total energy of the pristine monolayer, E_{Li} is the energy of an isolated Li atom and x refers to the Li concentration, for all four materials are given in Table III. The Li adsorption energy is higher for T' phase as compared to the H phase. For $Li_{0.5}MX_2$, the adsorption energy is largest for WSe_2 at −1.03 eV followed by $MoSe_2$ and MoS_2 at −0.99 and −0.97 eV/f.u., respectively, and smallest for WS_2 at −0.85 eV/f.u. This energy is comparable to the energy barrier to the phase transition at this Li concentration. For Li_1MX_2, the adsorption energy per MX_2 approximately doubles, to at least 2.5 times the energy barrier. If some of this energy is used to overcome the barrier to the transition, Li adsorption may be sufficient to make the process spontaneous. Furthermore, given that the rate of transition decreases exponentially with activation energy (as per the Arrhenius equation), we can conclude that, for a given X, WX_2 will transition at a slightly higher rate than MoX_2. Likewise, for a given M, MSe_2 will transition at a higher rate than MS_2.

This is contradictory to the observation of a higher percentage of T' phase found for WS_2 compared to $MoSe_2$ and WSe_2. To explain this, we must also consider the fact that in order to measure the T/H ratio experimentally, the exfoliated monolayers are washed with deionized water and dried in vacuum. In this process the Li ions desorb and the monolayers revert to their neutral state. They are prevented from transitioning immediately back to the ground-state H phase by an energy barrier. This is supported by the observation of the M^{4+} oxidation state in x-ray photoelectron spectra (XPS) [24,25,57].

The barriers for the reverse transition from the neutral T' phase to the neutral H phase, shown in Fig. 2, are now relevant. For all materials, the barrier to return directly to

the H phase is prohibitively high, ranging between 0.90 and 0.99 eV. Instead, the barrier to transition to a mixed T'' type phase is significantly lower, ranging between 0.39 and 0.48 eV. Experimental evidence for such an indirect transition from the T' phase back to the H phase for MoS_2 via a mixed T'' mixed phase can be found: By fitting the rate equation to *in situ* Raman measurements, the barrier to transform from the metastable metallic phase to the ground state was found to be 400 meV [17]. This barrier value is consistent with the calculated barrier to transition from the T'' mixed phase to the H phase of 450 meV calculated here (cf. Fig. 2), whereas the barrier to transition from the T' phase back to the H phase directly is 970 meV. This suggests that the transition from the T' phase to the H phase occurs in two steps for this material, via the T'' mixed phase.

The barrier to transition from the T'' mixed phase to the H phase is smallest for the two selenium compounds at 0.23 and 0.27 eV for $MoSe_2$ and WSe_2, respectively. The barrier for WS_2 is twice as high, at 0.49 eV. The significance of this difference in barrier for WS_2 and WSe_2 can be determined by calculating the exponential factor of the Arrhenius equation at room temperature ($k_B T = 25.7$ meV). This is of the order of 5×10^{-9} for WS_2, whereas it is of the order of 1×10^{-4} for WSe_2. This rate difference is significant and its effects should be experimentally observable. This can explain the significant difference between the percentage of T' phase observed in WS_2 compared to both $MoSe_2$ and WSe_2 [24]. However, the calculated activation barriers cannot explain the low $1T/2H$ ratio found in exfoliated MoS_2. This discrepancy could be due to nonelectronic effects, such as a poor exfoliation efficiency in certain organometallic compounds, edge effects related to the change in lateral size of the exfoliated monolayers, the presence of defects, or the oxidation of the exfoliated layers. Another possibility is that the simplified phase transition mechanism considered here does not consider the full nucleation process.

Finally, we note that the T'' mixed phase comprises of alternating H and T' phases, each a unit cell thick, as illustrated in Fig. 1. However, this phase can be viewed as just one example of a family of mixed T' and H phase structures. By changing the $T':H$ ratio in MoS_2 from 1:1 for the T'' structure to 2:1, the total energy difference between it and the H phase increases from 0.49 to 0.51 eV. By increasing the ratio further to 3:1, the energy difference increases further to 0.52 eV. Clearly the total energy of MoS_2 is strongly dependent upon the fraction of H phase. The energy of all such families of confined structures will be higher than that of the H phase but lower than that of the T' phase. The exact composition of such confined structures will be dependent on the available energy and the TMD flake size and shape and are not confined to the idealized one-dimensional structures discussed here. Experimentally, the boundary between the H phase and T' phase areas are observed to be atomically sharp, as in the T'' mixed phase. This boundary evolves over time via a transversal displacement of one of the S planes [13,62] leading to the complete phase transition of the flake. The observed partial phases, with mixed metallic (T') and insulating (H) regions, can be understood as intermediate stable structures which have lower barriers of transition.

V. CONCLUSION

Group-VI TMDs are known to undergo structural phase transitions from a semiconducting H phase to a metallic T phase when subjected to alkali metal assisted exfoliation. The efficiency of this process is strongly dependent on the chemical composition of the material. We show that the ratio of T' to H phase is maximized if the charge-induced transition from the H phase to the T' phase is favorable and the reverse transition upon removal of charge is unfavorable. For example, the high proportion of T phase found in WS_2 monolayers after alkali treatment can be explained by a high barrier to revert back to the H phase after the initial phase transition has been induced. While charged MSe_2 materials have the lowest energy barriers to the phase transition, the barriers to revert back to the H phase are also low. This can explain the relatively low content of metallic phase found in $MoSe_2$ and WSe_2 after exfoliation. Finally, the low proportion of metallic phase found in MoS_2 monolayers in some experiments cannot be explained using the activation barriers alone and so nonelectronic effects, such as a differing exfoliation efficiency or differing levels of monolayer oxidation, must also contribute to the outcome.

APPENDIX: IMPLICIT CHARGING

We highlight here some issues related to statically charging monolayers or slabs in DFT with periodic boundary conditions, as it is to these issues that we attribute the wide range of values reported in the literature for the critical charge required to induce a structural phase transition in TMDs.

For the case of isolated charged slabs, such as the TMD monolayers considered here, the electric field due to the extra uniform charge density is constant and should result in a potential that varies linearly with distance from the surface of the slab. When periodic boundary conditions are implemented, this linear potential is replaced by the combined effective potential due to the consecutive periodic images. The quantities relating to the isolated slabs can be recovered from these periodic calculations by applying a correction term to the effective potential and total energy. The exact functional form of this potential is discussed in detail by Andreussi *et al.* [63]. As discussed in the manual for VASP (in the section Monopole, Dipole and Quadrupole corrections) the leading term of this correction, which cancels the interaction of the linear potential with the background compensating charge, is absent. As a result, the total energy is essentially incorrect and cannot be relied upon.

Furthermore, we find that above a certain critical charge, positive eigenvalues are occupied. This was previously shown to occur for atomic anions and can be attributed to the self-interaction error [64].
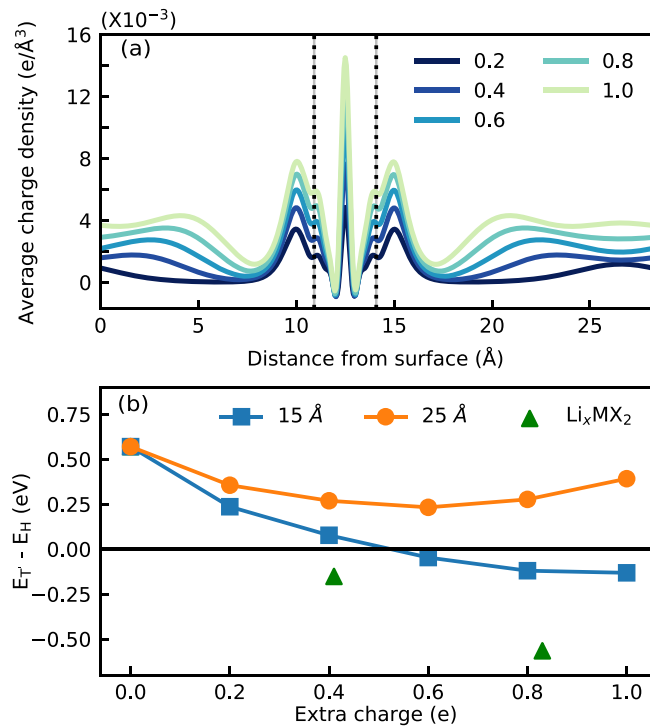
FIG. 4. (a) Planar average of the charge density across the TMD monolayers showing charge leakage into the vacuum region for typical values of excess charge. The positions of the chalcogen atoms are marked by black dashed lines. (b) The energy difference between the T' and the H phase of MoS_2 as a function of excess static charge for two different vacuum thickness, compared to the values found by explicitly charging the slab using Li atoms.

Finally, Topsakal *et al.* showed that, when the basis set is present in the vacuum region, excess negative charge does not stay on the slab but spills over in the vacuum, beyond a critical value which depends on the vacuum thickness [65]. This phenomenon is demonstrated in Fig. 4(a) for the H phase of MoS_2 with a vacuum length of 25 Å perpendicular to the surface of the slab and was previously shown for graphene [66]. The excess charge density added is placed in the vacuum and on the outer faces of the monolayer rather than on the d orbital of the metal atom.

To illustrate how these issues affect the determination of the critical charge required to induce a structural phase transition, we show in Fig. 4(b) the total energy difference between the H and the T' phase of MoS_2 as a function of excess charge, and for two different vacuum lengths. All three sources of error are now present, namely charge has spilled into the vacuum (above a certain critical excess charge value), the appropriate monopole correction is absent and positive eigenvalues are occupied. We find that the vacuum length of 15 Å (blue squares) shows a phase transition for excess charge of around $0.5e$/f.u. On increasing the vacuum length to 25 Å (orange circles) no such transition is observed.

Clearly it is not possible to get physically meaningful results using statically charged slabs combined with periodic boundary conditions using the current implementation of VASP (V5.4.1). A similar erroneous dependence on the vacuum length was also reported by Bal *et al.* for adsorbed molecules on charged surfaces, further highlighting the irreproducibility of such results [67]. These problems can be mitigated by applying correct boundary conditions when calculating the Hartree potential [68–72].

[1] S. Manzeli, D. Ovchinnikov, D. Pasquier, O. V. Yazyev, and A. Kis, 2D transition metal dichalcogenides, Nat. Rev. Mater. **2**, 17033 (2017).

[2] F. Ma, G. Gao, Y. Jiao, Y. Gu, A. Bilic, H. Zhang, Z. Chen, and A. Du, Predicting a new phase (T″) of two-dimensional transition metal di-chalcogenides and strain-controlled topological phase transition, Nanoscale **8**, 4969 (2016).

[3] M. A. Py and R. R. Haering, Structural destabilization induced by lithium intercalation in MoS_2 and related compounds, Can. J. Phys. **61**, 76 (1983).

[4] M. Kertesz and R. Hoffmann, Octahedral vs trigonal-prismatic coordination and clustering in transition-metal dichalcogenides, J. Am. Chem. Soc. **106**, 3453 (1984).

[5] X. Chia and M. Pumera, Layered transition metal dichalcogenide electrochemistry: Journey across the periodic table, Chem. Soc. Rev. **47**, 5602 (2018).

[6] D. Voiry, A. Mohite, and M. Chhowalla, Phase engineering of transition metal dichalcogenides, Chem. Soc. Rev. **44**, 2702 (2015).

[7] F. R. Gamble, Ionicity, atomic radii, and structure in the layered dichalcogenides of group IVb, Vb, and VIb transition metals, J. Solid State Chem. **9**, 358 (1974).

[8] L. Wang, Z. Xu, W. Wang, and X. Bai, Atomic mechanism of dynamic electrochemical lithiation processes of MoS_2 nanosheets, J. Am. Chem. Soc. **136**, 6693 (2014).

[9] B. Lei, Y. Pan, Z. Hu, J. Zhang, D. Xiang, Y. Zheng, R. Guo, C. Han, L. Wang, J. Lu *et al.*, Direct observation of semiconductor–metal phase transition in bilayer tungsten diselenide induced by potassium surface functionalization, ACS Nano **12**, 2070 (2018).

[10] F. Raffone, C. Ataca, J. C. Grossman, and G. Cicero, MoS_2 enhanced T-phase stabilization and tunability through alloying, J. Phys. Chem. Lett. **7**, 2304 (2016).

[11] S. Kretschmer, H.-P. Komsa, P. Bøggild, and A. V. Krasheninnikov, Structural transformations in two-dimensional transition-metal dichalcogenide MoS_2 under an electron beam: Insights from first-principles calculations, J. Phys. Chem. Lett. **8**, 3061 (2017).

[12] M. Pizzochero and O. V. Yazyev, Point defects in the $1T'$ and $2H$ phases of single-layer MoS_2: A comparative first-principles study, Phys. Rev. B **96**, 245402 (2017).

[13] Y.-C. Lin, D. O. Dumcenco, Y.-S. Huang, and K. Suenaga, Atomic mechanism of the semiconducting-to-metallic phase transition in single-layered MoS_2, Nat. Nanotechnol. **9**, 391 (2014).

[14] S. Cho, S. Kim, J. H. Kim, J. Zhao, J. Seok, D. H. Keum, J. Baik, D.-H. Choe, K. J. Chang, K. Suenaga *et al.*, Phase patterning for ohmic homojunction contact in $MoTe_2$, Science **349**, 625 (2015).

[15] Y. Kang, S. Najmaei, Z. Liu, Y. Bao, Y. Wang, X. Zhu, N. J. Halas, P. Nordlander, P. M. Ajayan, J. Lou *et al.*, Plasmonic hot electron induced structural phase transition in a MoS_2 monolayer, Adv. Mater. **26**, 6467 (2014).

[16] X. Fan, P. Xu, D. Zhou, Y. Sun, Y. C. Li, M. A. T. Nguyen, M. Terrones, and T. E. Mallouk, Fast and efficient preparation of exfoliated 2H MoS_2 nanosheets by sonication-assisted lithium intercalation and infrared laser-induced 1T to 2H phase reversion, Nano Lett. **15**, 5956 (2015).

[17] Y. Guo, D. Sun, B. Ouyang, A. Raja, J. Song, T. F. Heinz, and L. E. Brus, Probing the dynamics of the metallic-to-semiconducting structural phase transformation in MoS_2 crystals, Nano Lett. **15**, 5081 (2015).

[18] B. Radisavljevic and A. Kis, Mobility engineering and a metal–insulator transition in monolayer MoS_2, Nat. Mater. **12**, 815 (2013).

[19] Y. Wang, J. Xiao, H. Zhu, Y. Li, Y. Alsaid, K. Y. Fong, Y. Zhou, S. Wang, W. Shi, Y. Wang *et al.*, Structural phase transition in monolayer $MoTe_2$ driven by electrostatic doping, Nature (London) **550**, 487 (2017).

[20] M. Acerce, D. Voiry, and M. Chhowalla, Metallic 1T Phase MoS_2 nanosheets as supercapacitor electrode materials, Nat. Nanotechnol. **10**, 313 (2015).

[21] A. Nourbakhsh, A. Zubair, R. N. Sajjad, A. Tavakkoli KG, W. Chen, S. Fang, X. Ling, J. Kong, M. S. Dresselhaus, E. Kaxiras *et al.*, MoS_2 field-effect transistor with sub-10 nm channel length, Nano Lett. **16**, 7798 (2016).

[22] A. L. Friedman, F. K. Perkins, A. T. Hanbicki, J. C. Culbertson, and P. M. Campbell, Dynamics of chemical vapor sensing with MoS_2 using 1T/2H phase contacts/channel, Nanoscale **8**, 11445 (2016).

[23] J. Luxa, P. Vosecký, V. Mazánek, D. Sedmidubský, M. Pumera, and Z. Sofer, Cation-controlled electrocatalytical activity of transition-metal disulfides, ACS Catal. **8**, 2774 (2018).

[24] A. Ambrosi, Z. Sofer, and M. Pumera, $2H \rightarrow 1T$ phase transition and hydrogen evolution activity of MoS_2, $MoSe_2$, WS_2, and WSe_2 strongly depends on the MX_2 composition, Chem. Commun. **51**, 8450 (2015).

[25] N. Rohaizad, C. C. Mayorga-Martinez, Z. Sofer, and M. Pumera, 1T-phase transition metal dichalcogenides (MoS_2, $MoSe_2$, WS_2, and WSe_2) with fast heterogeneous electron transfer: Application on second-generation enzyme-based biosensor, ACS Appl. Mater. Int. **9**, 40697 (2017).

[26] S. M. Tan, Z. Sofer, J. Luxa, and M. Pumera, Aromatic-exfoliated transition metal dichalcogenides: Implications for inherent electrochemistry and hydrogen evolution, ACS Catal. **6**, 4594 (2016).

[27] Y. Li, K.-A. N. Duerloo, K. Wauson, and E. J. Reed, Structural semiconductor-to-semimetal phase transition in two-dimensional materials induced by electrostatic gating, Nat. Commun. **7**, 10671 (2016).

[28] X. Sun, Z. Wang, Z. Li, and Y. Q. Fu, Origin of structural transformation in mono-and bi-layered molybdenum disulfide, Sci. Rep. **6**, 26666 (2016).

[29] G. Gao, Y. Jiao, F. Ma, Y. Jiao, E. Waclawik, and A. Du, Charge mediated semiconducting-to-metallic phase transition in molybdenum disulfide monolayer and hydrogen evolution reaction in new 1T′ phase, J. Phys. Chem. C **119**, 13124 (2015).

[30] G. Kresse and J. Furthmüller, Efficiency of *ab-initio* total energy calculations for metals and semiconductors using a plane-wave basis set, Comput. Mater. Sci. **6**, 15 (1996).

[31] G. Kresse and J. Furthmüller, Efficient iterative schemes for *ab initio* total-energy calculations using a plane-wave basis set, Phys. Rev. B **54**, 11169 (1996).

[32] G. Kresse and D. Joubert, From ultrasoft pseudopotentials to the projector augmented-wave method, Phys. Rev. B **59**, 1758 (1999).

[33] J. Klimeš, D. R. Bowler, and A. Michaelides, Van der Waals density functionals applied to solids, Phys. Rev. B **83**, 195131 (2011).

[34] M. Dion, H. Rydberg, E. Schröder, D. C. Langreth, and B. I. Lundqvist, Van der Waals Density Functional for General Geometries, Phys. Rev. Lett. **92**, 246401 (2004).

[35] T. Björkman, Testing several recent van der Waals density functionals for layered structures, J. Chem. Phys. **141**, 074708 (2014).

[36] U. Patil and N. M. Caffrey, Adsorption of common solvent molecules on graphene and MoS_2 from first-principles, J. Chem. Phys. **149**, 094702 (2018).

[37] G. Henkelman, B. P. Uberuaga, and H. Jónsson, A climbing image nudged elastic band method for finding saddle points and minimum energy paths, J. Chem. Phys. **113**, 9901 (2000).

[38] G. Henkelman and H. Jónsson, Improved tangent estimate in the nudged elastic band method for finding minimum energy paths and saddle points, J. Chem. Phys. **113**, 9978 (2000).

[39] R. A. Gordon, D. Yang, E. D. Crozier, D. T. Jiang, and R. F. Frindt, Structures of exfoliated single layers of WS_2, MoS_2, and $MoSe_2$ in aqueous suspension, Phys. Rev. B **65**, 125407 (2002).

[40] J. Heising and M. G. Kanatzidis, Structure of restacked MoS_2 and WS_2 elucidated by electron crystallography, J. Am. Chem. Soc. **121**, 638 (1999).

[41] J. C. Wildervanck and F. Jellinek, Preparation and crystallinity of molybdenum and tungsten sulfides, Z. Anorg. Allg. Chem. **328**, 309 (1964).

[42] B. Schönfeld, J. J. Huang, and S. C. Moss, Anisotropic mean-square displacements (MSD) in single-crystals of 2H- and 3R-MoS_2, Acta Crystallogr. Sect. B **39**, 404 (1983).

[43] K. D. Bronsema, J. L. De Boer, and F. Jellinek, On the structure of molybdenum diselenide and disulfide, Z. Anorg. Allg. Chem. **540**, 15 (1986).

[44] W. J. Schutte, J. L. De Boer, and F. Jellinek, Crystal structures of tungsten disulfide and diselenide, J. Solid State Chem. **70**, 207 (1987).

[45] R. G. Dickinson and L. Pauling, The crystal structure of molybdenite, J. Am. Chem. Soc. **45**, 1466 (1923).

[46] R. E. Bell and R. E. Herfert, Preparation and characterization of a new crystalline form of molybdenum disulfide, J. Am. Chem. Soc. **79**, 3351 (1957).

[47] N. V. Podberezskaya, S. A. Magarill, N. V. Pervukhina, and S. V. Borisov, Crystal chemistry of dichalcogenides MX_2, J. Struct. Chem. **42**, 654 (2001).

[48] M. Samadi, N. Sarikhani, M. Zirak, H. Zhang, H.-L. Zhang, and A. Z. Moshfegh, Group 6 transition metal dichalcogenide nanomaterials: Synthesis, applications and future perspectives, Nanoscale Horizons **3**, 90 (2018).

[49] A. Kumar and P. K. Ahluwalia, Electronic structure of transition metal dichalcogenides monolayers 1H-MX_2 (M= Mo, W; X= S, Se, Te) from *ab-initio* theory: New direct band gap semiconductors, Eur. Phys. J. B **85**, 186 (2012).

[50] J. Gusakova, X. Wang, L. L. Shiau, A. Krivosheeva, V. Shaposhnikov, V. Borisenko, V. Gusakov, and B. K. Tay, Electronic properties of bulk and monolayer TMDs: Theoretical study within DFT framework (GVJ-2e method), Phys. Status Solidi (a) **214**, 1700218 (2017).

[51] G.-B. Liu, W.-Yu. Shan, Y. Yao, W. Yao, and D. Xiao, Three-band tight-binding model for monolayers of group-VIB transition metal dichalcogenides, Phys. Rev. B **88**, 085433 (2013).

[52] Á. García, E. del Corro, M. Kalbac, and O. Frank, Tuning the electronic properties of monolayer and bilayer transition metal dichalcogenide compounds under direct out-of-plane compression, Phys. Chem. Chem. Phys. **19**, 13333 (2017).

[53] I. S. Kwon, I. H. Kwak, H. G. Abbas, G. Jung, Y. Lee, J. Park, S. J. Yoo, J.-G. Kim, and H. S. Kang, Intercalation of aromatic amine for the 2H–1T' phase transition of MoS_2 by experiments and calculations, Nanoscale **10**, 11349 (2018).

[54] D. Nasr Esfahani, O. Leenaerts, H. Sahin, B. Partoens, and F. M. Peeters, Structural transitions in monolayer MoS_2 by lithium adsorption, J. Phys. Chem. C **119**, 10602 (2015).

[55] M. Kan, J. Y. Wang, X. W. Li, S. H. Zhang, Y. W. Li, Y. Kawazoe, Q. Sun, and P. Jena, Structures and phase transition of a MoS_2 monolayer, J. Phys. Chem. C **118**, 1515 (2014).

[56] K. Leng, Z. Chen, X. Zhao, W. Tang, B. Tian, C. T. Nai, W. Zhou, and K. P. Loh, Phase restructuring in transition metal dichalcogenides for highly stable energy storage, ACS Nano **10**, 9208 (2016).

[57] Q. Li, Z. Yao, J. Wu, S. Mitra, S. Hao, T. S. Sahu, Y. Li, C. Wolverton, and V. P. Dravid, Intermediate phases in sodium intercalation into MoS_2 nanosheets and their implications for sodium-ion batteries, Nano Energy **38**, 342 (2017).

[58] C. A. Papageorgopoulos and W. Jaegermann, Li intercalation across and along the van der Waals surfaces of MoS_2 (0001), Surf. Sci. **338**, 83 (1995).

[59] J. Hong, Y. Pan, Z. Hu, D. Lv, C. Jin, W. Ji, J. Yuan, and Z. Zhang, Direct imaging of kinetic pathways of atomic diffusion in monolayer molybdenum disulfide, Nano Lett. **17**, 3383 (2017).

[60] W. Tang, E. Sanville, and G. Henkelman, A grid-based Bader analysis algorithm without lattice bias, J. Phys.: Condens. Matter **21**, 084204 (2009).

[61] A. N. Enyashin and G. Seifert, Density-functional study of Li_xMoS_2 intercalates ($0 \leqslant x \leqslant 1$), Comput. Theor. Chem. **999**, 13 (2012).

[62] Q. Jin, N. Liu, B. Chen, and D. Mei, Mechanisms of semiconducting 2H to metallic 1T phase transition in two-dimensional MoS_2 nanosheets, J. Phys. Chem. C **122**, 28215 (2018).

[63] O. Andreussi and N. Marzari, Electrostatics of solvated systems in periodic boundary conditions, Phys. Rev. B **90**, 245101 (2014).

[64] M.-C. Kim, E. Sim, and K. Burke, Communication: Avoiding unbound anions in density functional calculations, J. Chem. Phys. **134**, 171103 (2011).

[65] M. Topsakal and S. Ciraci, Effects of static charging and exfoliation of layered crystals, Phys. Rev. B **85**, 045121 (2012).

[66] M. Topsakal and S. Ciraci, Static charging of graphene and graphite slabs, Appl. Phys. Lett. **98**, 131908 (2011).

[67] K. M. Bal and E. C. Neyts, Modelling molecular adsorption on charged or polarized surfaces: A critical flaw in common approaches, Phys. Chem. Chem. Phys. **20**, 8456 (2018).

[68] T. Brumme, M. Calandra, and F. Mauri, First-principles theory of field-effect doping in transition-metal dichalcogenides: Structural properties, electronic structure, Hall coefficient, and electrical conductivity, Phys. Rev. B **91**, 155436 (2015).

[69] T. Sohier, M. Calandra, and F. Mauri, Density functional perturbation theory for gated two-dimensional heterostructures: Theoretical developments and application to flexural phonons in graphene, Phys. Rev. B **96**, 075448 (2017).

[70] M. Otani and O. Sugino, First-principles calculations of charged surfaces and interfaces: A plane-wave nonrepeated slab approach, Phys. Rev. B **73**, 115407 (2006).

[71] M. H. Bani-Hashemian, S. Brück, M. Luisier, and J. VandeVondele, A generalized Poisson solver for first-principles device simulations, J. Chem. Phys. **144**, 044113 (2016).

[72] T. Gunst, K. Kaasbjerg, and M. Brandbyge, Flexural-Phonon Scattering Induced by Electrostatic Gating in Graphene, Phys. Rev. Lett. **118**, 046601 (2017).